GEOPHYSICS, VOL. 71, NO. 4 (JULY-AUGUST 2006); P. D135–D143, 17 FIGS.
10.1190/1.2212274

PS-wave moveout inversion for tilted TI media: A physical-modeling study

Pawan Dewangan[1], Ilya Tsvankin[2], Mike Batzle[3], Kasper van Wijk[4], and Matthew Haney[5]

ABSTRACT

Mode-converted PS-waves can provide critically important information for velocity analysis in transversely isotropic (TI) media. We demonstrate, with physical-modeling data, that the combination of long-spread reflection traveltimes of PP- and PS-waves can be inverted for the parameters of a horizontal TI layer with a tilted symmetry axis. The 2D multicomponent reflection data are acquired over a phenolic sample manufactured to simulate the effective medium formed by steeply dipping fracture sets or shale layers.

The reflection moveout of PS-waves in this model is asymmetric with respect to the source and receiver positions, and the moveout-asymmetry attributes play a crucial role in constraining the TI parameters. Applying the modified PP + PS = SS method to the PP and PS traveltimes recorded in the symmetry-axis plane, we compute the time and offset asymmetry attributes of the PS-waves along with the traveltimes of the pure SS reflections. The algorithm of Dewangan and Tsvankin is then used to invert the combination of the moveout attributes of PP-, SS-, and PS-waves for the medium parameters and the thickness of the sample. It should be emphasized that the pure-mode (PP and SS) traveltimes alone are insufficient for the inversion, even if 3D wide-azimuth data are available.

Our estimates of the symmetry axis tilt and layer thickness almost coincide with the actual values. The inverted model is also validated by reproducing the results of transmission experiments with both P- and S-wave sources. The transmitted SV wavefield exhibits a prominent cusp (triplication) accurately predicted by the parameter-estimation results.

INTRODUCTION

Transverse isotropy (TI) is a common anisotropic symmetry usually associated with shaly sediments, fine layering on a small scale compared to seismic wavelength, or aligned penny-shaped cracks (e.g., Thomsen, 1986; Helbig, 1994). In active tectonic areas, such as fold-and-thrust belts, the symmetry axis of TI formations is often tilted away from the vertical. Such tilted transversely isotropic (TTI) models are typical of the Canadian Foothills, where they cause significant mispositioning of imaged reflectors (e.g., Isaac and Lawton, 1999; Vestrum et al., 1999). An effective TTI medium also describes a system of parallel, dipping, penny-shaped cracks embedded in isotropic host rock (Angerer et al., 2002), as well as progradational sequences.

While conventional migration algorithms can be readily extended to handle transverse isotropy, parameter estimation for TTI media remains a challenging problem. Grechka and Tsvankin (2000) show that P-wave reflection moveout alone does not constrain the parameters of a horizontal TTI layer, even if a wide range of source-receiver azimuths are available. Furthermore, supplementing P-wave data with wide-azimuth SV-wave traveltimes is still insufficient to make the inversion unique (Grechka and Tsvankin, 2000; Grechka et al., 2002).

Important information for velocity analysis in TTI media is provided by mode-converted PS (PSV) data. Because of the deviation of the symmetry axis from both vertical and horizontal directions, the moveout of PS-waves reflected from horizontal interfaces becomes asymmetric (i.e., the PS-wave traveltime does not stay the same if the source and receiver are interchanged). As demonstrated by Dewangan and Tsvankin (2006a), moveout-asymmetry attributes of PS-waves can help estimate all parameters of a horizontal TTI layer using solely reflection data. The algorithm of Dewangan and

Manuscript received by the Editor July 11, 2005; revised manuscript received October 7, 2005; published online August 9, 2006.
[1]Formerly Colorado School of Mines, Center for Wave Phenomena, Department of Geophysics, Golden, Colorado 80401; presently National Institute of Oceanography, Geological Oceanography Division, Dona Paul, Goa-403004, India. E-mail: pdewangan@darya.nio.org.
[2]Colorado School of Mines, Center for Wave Phenomena, Department of Geophysics, 1500 Illinois Street, Golden, Colorado 80401. E-mail: ilya@dix.mines.edu.
[3]Colorado School of Mines, Center for Rock Abuse, Department of Geophysics, Golden, Colorado 80401. E-mail: mbatzle@mines.edu.
[4]Colorado School of Mines, Physical Acoustics Laboratory, Department of Geophysics, Golden, Colorado 80401. E-mail: kasper@acoustics.mines.edu.
[5]Formerly Colorado School of Mines, Center for Wave Phenomena, Department of Geophysics, Golden, Colorado 80401; presently Sandia National Laboratories, Geophysical Technology Department, Albuquerque, New Mexico 87185. E-mail: mmhaney@sandia.gov.

Tsvankin (2006a), based on a modification of the so-called PP + PS = SS method (Grechka and Tsvankin, 2002; Grechka and Dewangan, 2003), operates with long-offset PP and PS reflections acquired in the vertical plane that contains the symmetry axis (the *symmetry-axis plane*).

We show on physical-modeling data that the combination of PP and PS reflection traveltimes can indeed constrain all parameters of a horizontal TTI layer. Multicomponent, multioffset reflection seismic lines are acquired in the symmetry-axis plane of a phenolic sample to record long-spread moveouts of PP- and PS(PSV)-waves. Following the methodology of Dewangan and Tsvankin (2006a), the modified PP + PS = SS method is used to compute pure SS-wave reflection traveltimes and the asymmetry attributes of PS-waves. Moveout asymmetry information is then combined with the pure-mode (PP and SS) normal-moveout (NMO) velocities and zero-offset traveltimes to estimate the model parameters. Accuracy of the inverted TTI model is verified by matching the measured PP and PS traveltimes and reproducing the results of transmission experiments.

EXPERIMENTAL SETUP

Physical models have been used in geophysics for many years. Early work provided basic *seismic* data sets because computational techniques were too slow. More recent research has focused on specific problems, geometries, or attributes. For example, Ebrom et al. (1992) investigated the influence of 3D wave-propagation phenomena on 2D seismic data (e.g., sideswipe), Rathore et al. (1995) measured the acoustic properties and anisotropy parameters of synthetic sandstones containing artificial cracks with selected geometries and densities, and Isaac and Lawton (1999) demonstrated that the presence of TTI layers above the target may cause significant distortions in conventional isotropic imaging. Such models make it possible to produce data influenced by a range of realistic physical factors (noise, interference, band limitations, etc.) under known conditions and medium geometries. At the same time, physical modeling has a number of limitations related to measurement procedures, fabrication, and size restrictions (e.g., inconsistent coupling, imperfect shape or component bonding, end effects).

To simulate a TTI layer, we used XX-paper-based phenolic composed of thin layers of paper bonded with phenolic resin. This fine layering causes effective anisotropy in the long-wavelength limit; also, phenolic itself is known to have either TI or orthorhombic symmetry (Grechka et al., 1999; Isaac and Lawton, 1999). The sample was prepared by cutting a large block of commercially available phenolic into smaller blocks and pasting them together at an angle to form a TTI medium (Figure 1). To simulate steeply dipping fractures similar to those identified by Angerer et al. (2002) on field data, the tilt ν of the symmetry axis from the vertical was chosen to be 70° (Figure 2). This physical model can also describe reflections from a horizontal interface overlain by a sequence of dipping shale layers (e.g., Vestrum et al., 1999).

The experiments were conducted at the Center for Rock Abuse and in the Physical Acoustics Laboratory at Colorado School of Mines (CSM). Measurements (reflection and transmission surveys) were made only in the symmetry-axis plane of the sample, where the velocities and polarizations are described by TI equations, even if the medium as a whole has orthorhombic symmetry. One reflection survey was acquired using source and receiver transducers (flat-faced cylindrical piezoelectric ultrasonic contact transducers). To excite P-waves, the source transducer was polarized vertically; for shear (SV) waves we used a horizontal transducer.

Another reflection survey, as well as transmission data, were generated by the source transducer and recorded with a scanning laser vibrometer that measures the absolute particle velocity on the surface of the sample via the Doppler shift (Nishizawa et al., 1997; Scales and van Wijk, 1999). The records of multiple shots were stacked to improve data quality. The scanning head is programmed to move the beam after each measurement, so that dense arrays of data can be recorded automatically. Therefore, data acquisition with the laser vibrometer is much more efficient compared with time-consuming transducer measurements, where relatively large receivers have to be moved manually.

SEISMIC REFLECTION EXPERIMENT

The inversion algorithm of Dewangan and Tsvankin (2006a) operates with PP- and PS-waves recorded in split-spread geometry and requires the offset-to-depth ratio to reach at least two. First, we acquired PP- and PS-wave shot gathers by fixing the P-wave shot transducer at one end of the model and manually moving the receiver transducer with an increment of 1 cm until the offset reached 30 cm, which corresponds to an offset-to-depth ratio of 2.8 (Figure 2). This procedure was repeated by placing the source transducer at the other end of the model to record negative offsets.

Because the sample is laterally homogeneous, shot gathers can be interpreted as common-midpoint (CMP) gathers. To verify that the lateral heterogeneity of the sample is negligible, we recorded a constant-offset P-wave section (Figure 3). The first arrival (the direct P-wave) and the P-wave multiple at a time of about 0.17 ms exhibit relatively weak traveltime and waveform variations along the line. The waveform of the P-wave primary recorded around 0.08 ms is distorted because of its interference with the ground roll. Minor lateral variations in the waveforms may also be related to errors in receiver positioning and to scattering on air bubbles between imperfectly glued blocks.

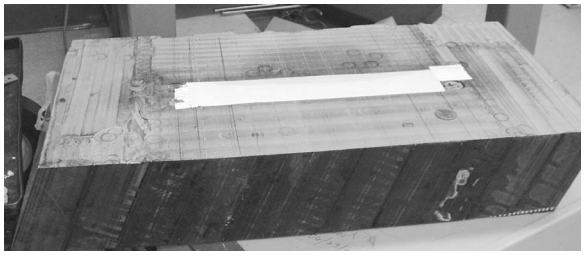

Figure 1. Physical model representing a horizontal TTI layer (with a U. S. quarter on top for scale). The dipping blocks are made of phenolic material.

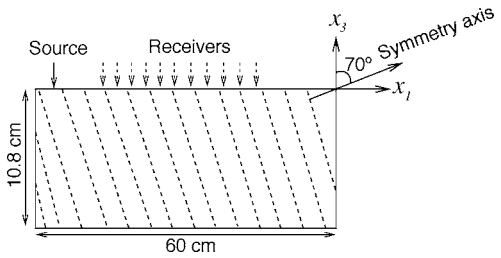

Figure 2. To simulate a reflection survey, the sources and receivers were placed on top of the sample in the symmetry-axis plane.

We then acquired another reflection survey by replacing the receiver transducer with the laser vibrometer. The sampling interval for the vibrometer dataset was 2 mm; the maximum offset-to-depth ratio was limited to 2.5 (the maximum offset was 27 cm).

PP-waves (vertical component)

For the vertical wavefield component recorded with the contact transducer (Figure 4a), the offset could not be smaller than 3 cm because of the finite transducer size. The minimum offset for the densely spaced data recorded with the laser vibrometer was 2 cm (Figure 4b). Because the vibrometer measures the particle velocity at a point, it is possible to record closer to the source, but the signal quality deteriorates at far offsets. The relatively poor quality of the long-offset vibrometer data may be related to the increasing contribution of the horizontal wavefield component and to technical problems with the recording equipment.

The two data sets in Figure 4 are quite similar, but identification of reflection events is hampered by their interference with the ground roll. To suppress the ground roll, we applied standard F-K dip filtering, which significantly improved the quality of the section (Figure 5). The first arrival is the direct P-wave traveling with a horizontal velocity close to 2620 m/s. The strong ground roll clearly visible in Figure 4 travels with a velocity of 1285 m/s, which is slightly smaller than the shear-wave velocity along the symmetry axis. The P-wave primary reflection from the bottom of the block and the first multiple can be identified at zero-offset times of 0.064 ms and 0.128 ms, respectively. Because the laser dataset is more densely sampled and has better coherency, we used it for manually picking the traveltimes of the primary reflection.

The dominant frequency of the P-wave data decreases from 200 kHz at near offsets to around 40 kHz at far offsets, which indicates that the medium is strongly attenuative (Figure 6). Assuming a dominant frequency of 100 kHz, the units of time and distance used in our experiment should be scaled (multiplied) by 5000 to obtain the corresponding values for seismic field data with a frequency of 20 Hz; the equivalent thickness of the layer would be 540 m.

To estimate the P-wave normal-moveout (NMO) velocity, we applied conventional hyperbolic velocity analysis (Figure 7). The influence of nonhyperbolic moveout was mitigated by muting out long offsets; the maximum offset-to-depth ratio used to compute the semblance in Figure 7a was close to one. The best-fit NMO velocity $V_{\mathrm{nmo},P}$, which flattens the near-offset primary and multiple reflections (Figure 7b), is 2350 ± 50 m/s. (The standard deviation in $V_{\mathrm{nmo},P}$ was computed from the scatter of traveltimes around the best-fit hyperbola.)

Because the NMO-corrected gather in Figure 7b is not flat at large offsets, the moveout curve is nonhyperbolic. This deviation from hyperbolic

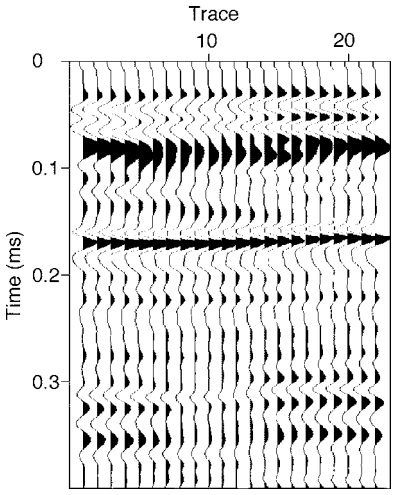

Figure 3. Constant-offset P-wave section acquired to validate the assumption of lateral homogeneity; the offset is 10 cm.

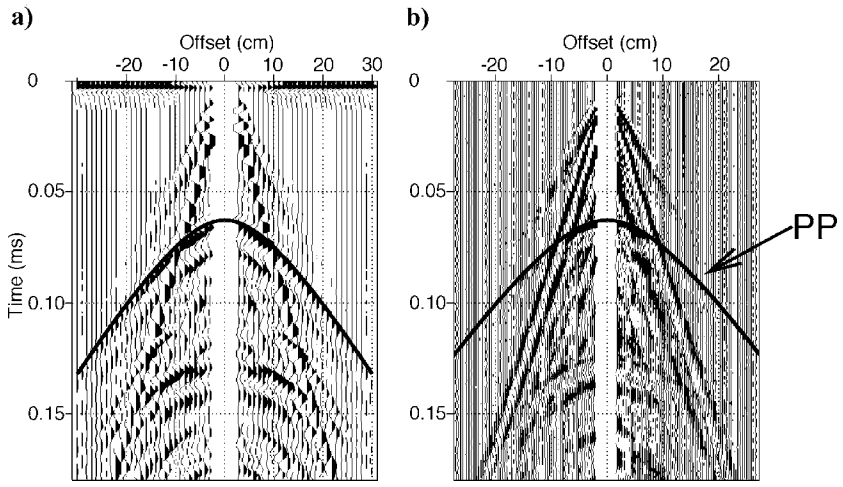

Figure 4. Vertical component of the wavefield generated by a vertical transducer. (a) Data recorded with the P-wave contact transducer; (b) densely sampled data recorded with the laser vibrometer. The first arrival is the direct P-wave; the PP-wave reflection from the bottom of the block (solid line) arrives at a zero-offset time of 0.064 ms.

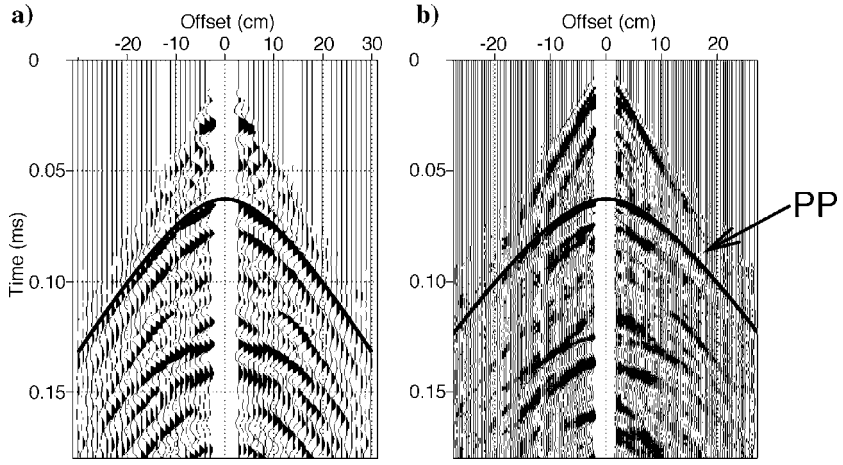

Figure 5. Data from Figure 4 after application of F-K filtering to suppress the ground roll.

moveout in a single homogeneous layer implies that the medium is anisotropic, and the anisotropy is not elliptical (e.g., Tsvankin, 2001).

The event arriving at $t_0 = 0.11$ ms in Figure 5 with a lower moveout velocity than that of the P-waves may be interpreted as a converted PS mode. Because the PS-wave polarization vector at small and moderate offsets is subhorizontal, this event is not prominent on the vertical component. To clearly identify mode-converted waves and pick their traveltimes, we carried out the experiments described in the next section.

Converted (PS and SP) waves

To acquire the converted PS(PSV)-wave, we recorded the wavefield from the vertical source transducer with a horizontal receiver transducer (Figure 8a). The geometry of this experiment was the same as the one used for recording the vertical wavefield component. We verified that there was almost no energy on the crossline (transverse) component, which indicates that the data were indeed acquired in a symmetry plane of the medium. Also, shear-wave splitting along the symmetry axis was negligible, suggesting that the model is either TI or a special case of orthorhombic media with equal anisotropy coefficients $\gamma^{(1)}$ and $\gamma^{(2)}$ (Tsvankin, 1997, 2001). Because of the kinematic equivalence between the symmetry planes of orthorhombic and TI media, the parameter-estimation algorithm of Dewangan and Tsvankin (2006a) is valid for both plausible models.

So far, the laser vibrometer system available at CSM has not been used to record the horizontal component of the wavefield. This limitation, however, can be overcome by recording mode-converted SP-waves and treating their traveltimes (according to reciprocity) as those of the corresponding PS-waves. A shear transducer served as the source and the laser vibrometer as the detector of the vertical wavefield component (Figure 8b). In the moveout analysis below, traveltimes of the acquired SP-wave were substituted for those of the PS-wave, although the sign of the SP-wave source-receiver offset was reversed when constructing a split-spread PS-wave gather (the source-receiver vectors for the SP and PS modes point in opposite directions).

Both acquired sections, after application of F-K filtering, are displayed in Figure 9. As was the case with the vertical component, there is close similarity between the two data sets recorded using different experimental setups. Moveout of the mode-converted PS- and SP-waves is strongly asymmetric, with a substantial difference between the traveltimes for positive and negative offsets (Figure 10). Because the model is laterally homogeneous, the PS-wave moveout asymmetry is caused entirely by the oblique orientation of the symmetry axis. Note that the moveout of converted waves is symmetric in any laterally homogeneous medium with a horizontal symmetry plane, including TI models with a vertical (VTI) and horizontal (HTI) symmetry axis (e.g., Tsvankin and Grechka, 2000).

Traveltime picks of the PS-wave, marked by the solid line in Figure 9, were made using the laser vibrometer dataset. Because of the moveout asymmetry, the minimum PS-wave traveltime is recorded at an offset of $x = 6$ cm; the wavelet reverses its polarity somewhere between zero offset and the traveltime minimum (Figure 10). To facilitate visual correlation of PS traveltimes, we removed this polarity reversal from Figures 8–10.

PP-wave primary reflection can be identified even on the horizontal component around the zero-offset time $t_{P0} = 0.064$ ms. It may also be possible to tentatively pick the SS-wave reflected arrival; but, as expected, in Figure 9 it is much weaker than the converted modes.

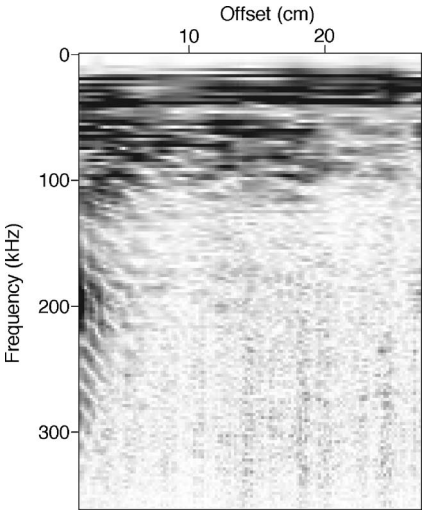

Figure 6. Amplitude spectra of the P-wave traces showing a decrease in frequency with offset.

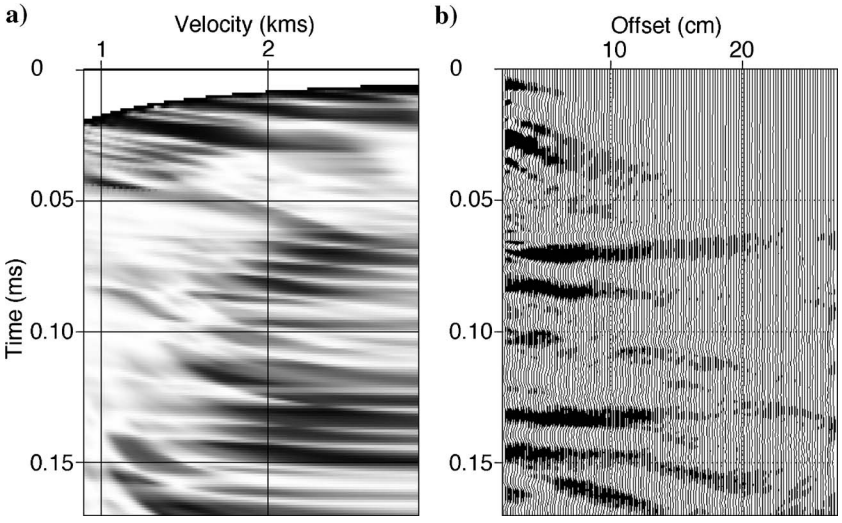

Figure 7. Conventional hyperbolic velocity analysis of the P-wave data. (a) Semblance panel computed for a maximum offset-to-depth ratio close to one; (b) the gather corrected for hyperbolic moveout using a moveout velocity of 2350 m/s.

Data processing

Reflection traveltimes of both the PP-wave and the converted wave were manually picked from the laser vibrometer datasets. To smooth the traveltimes and interpolate/extrapolate them at near offsets, we approximated both PP and PS (SP) moveouts with a sixth-order polynomial using the least-squares method.

The key processing step was application of the PP + PS = SS method suggested by Grechka and Tsvankin (2002) and Grechka and Dewangan

(2003) and modified in Dewangan and Tsvankin (2006a). The idea of this method is to identify two reciprocal PS-wave rays with the same reflection (conversion) point and combine their traveltimes with that of the PP-wave to compute the moveout of the SS-wave primary reflection. This can be accomplished by matching the reflection slopes on common-receiver gathers of PP- and PS-waves, as illustrated in Figure 11 (Grechka and Tsvankin, 2002). Because the PS rays recorded at points $x^{(3)}$ and $x^{(4)}$ have the same reflection point as the PP reflection $x^{(1)}Rx^{(2)}$, the traveltime τ_{SS} of the SS-wave (not physically excited in the survey) is determined from

$$\tau_{SS}(x^{(3)},x^{(4)}) = t_{PS}(x^{(1)},x^{(3)}) + t_{PS}(x^{(2)},x^{(4)}) - t_{PP}(x^{(1)},x^{(2)}), \quad (1)$$

where t_{PS} and t_{PP} are the traveltimes of the PS and PP reflections, respectively. Note that application of this technique requires correlating PP and PS reflection events and picking their traveltimes, although explicit velocity information is not needed.

Alternatively, PP and PS arrivals with the same reflection point can be identified by computing the time τ_{SS} in equation 1 for each desired SS-wave shot-receiver pair $(x^{(3)},x^{(4)})$ over a wide range of the coordinates $x^{(1)}$ and $x^{(2)}$ (Grechka and Dewangan, 2003; Dewangan and Tsvankin, 2006a):

$$\tau_{SS}(x^{(3)},x^{(4)}) = \min_{x^{(1)},x^{(2)}} (t_{PS}(x^{(1)},x^{(3)}) + t_{PS}(x^{(2)},x^{(4)}) - t_{PP}(x^{(1)},x^{(2)})). \quad (2)$$

The minimum of the function 2 in both the $x^{(1)}$- and $x^{(2)}$-directions corresponds to the P-wave sources that generate the reciprocal PS arrivals with the same reflection point. The value of τ_{SS} corresponding to this minimum yields the SS traveltime from $x^{(3)}$ to $x^{(4)}$.

We opted to employ the latter procedure to compute the SS-wave traveltime as a function of the SS-wave offset $x_{SS} = |x^{(3)} - x^{(4)}|$ (Figure 12). Then, conventional hyperbolic velocity analysis was applied to the constructed SS arrivals to estimate their stacking velocity ($V_{\mathrm{nmo},S}$ = 1780 m/s) and zero-offset traveltime (t_{S0} = 0.149 ms).

Next, we followed the methodology of Dewangan and Tsvankin (2006a) in computing the time and offset asymmetry attributes of the PS-wave:

$$\Delta t_{PS}(x^{(3)},x^{(4)}) = t_{PS}(x^{(1)},x^{(3)}) - t_{PS}(x^{(2)},x^{(4)}); \quad (3)$$

$$\Delta \mathbf{x}_{PS}(x^{(3)},x^{(4)}) = \mathbf{x}_{PS}(x^{(1)},x^{(3)}) + \mathbf{x}_{PS}(x^{(2)},x^{(4)}). \quad (4)$$

The time asymmetry attribute Δt_{PS} (Figure 13a) rapidly increases with offset and reaches about 20% of the zero-offset time. In contrast, the projection of the vector $\Delta \mathbf{x}_{PS}$ onto the x_1-axis (Δx_{PS}) reaches its maximum magnitude at small SS-wave offsets (Figure 13b), as predicted by the analytic results of Dewangan and Tsvankin (2006a) for the symmetry axis deviating by more than 45° from the vertical. Note that the attribute Δx_{PS} at zero offset ($x^{(3)} = x^{(4)}$) is twice the offset $x_{\min}$ corresponding to the minimum traveltime in the PS-wave CMP gather (Tsvankin and Grechka, 2000).

Parameter estimation

The vector **d** of input data for the inversion procedure includes the NMO velocities and zero-offset times of the PP- and SS-waves and the asymmetry attributes of the PS-wave:

$$\mathbf{d} \equiv \{V_{\mathrm{nmo},P}, t_{P0}, V_{\mathrm{nmo},S}, t_{S0}, \Delta t_{PS}(x_{SS}), \Delta x_{PS}(x_{SS})\}. \quad (5)$$

The analytic expressions needed to model these quantities are given in Dewangan and Tsvankin (2006a), where the offset $x_{\min}$ of the traveltime minimum was used instead of the asymmetry attribute

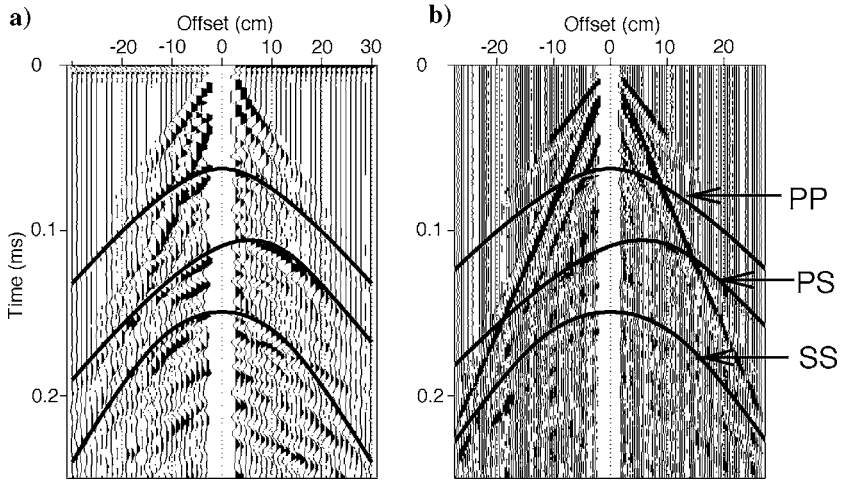

Figure 8. Data acquired with (a) the P-wave source transducer and S-wave receiver transducer; (b) the S-wave source transducer and the laser vibrometer as the receiver. Solid lines are the picked traveltimes. The converted wave from the bottom of the model has an asymmetric moveout curve with the apex at 0.11 ms. On both plots we reversed the polarity of mode-converted waves at negative offsets to remove the influence of the polarity reversals and facilitate traveltime picking.

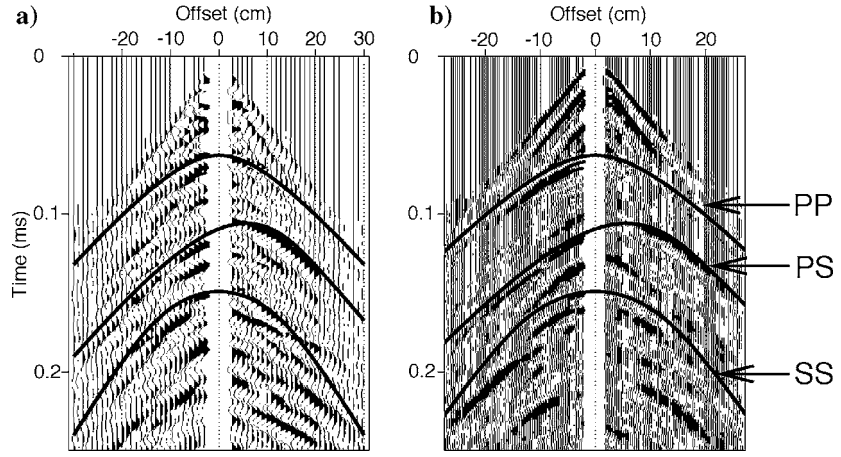

Figure 9. Data from Figure 8 after application of F-K filtering to suppress the ground roll.

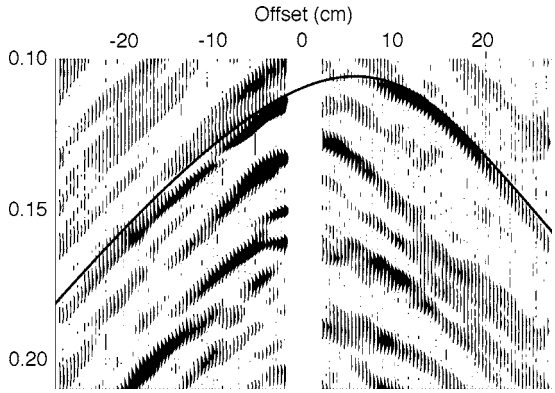

Figure 10. Asymmetric converted-wave gather from Figure 9b.

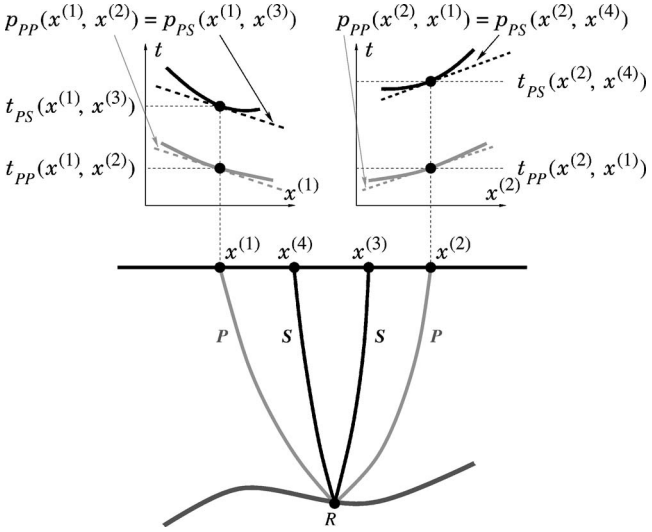

Figure 11. PP + PS = SS method is designed to find the source/receiver coordinates of the PP and PS rays with the same (albeit unknown) reflection point *R*. By matching the slopes on common-receiver gathers (i.e., the ray parameters) of the PP- and PS-waves, it is possible to estimate the recording locations $x^{(3)}$ and $x^{(4)}$ of the PS arrivals that have P-wave legs in common with the PP reflection from $x^{(1)}$ to $x^{(2)}$ (after Grechka and Tsvankin, 2002).

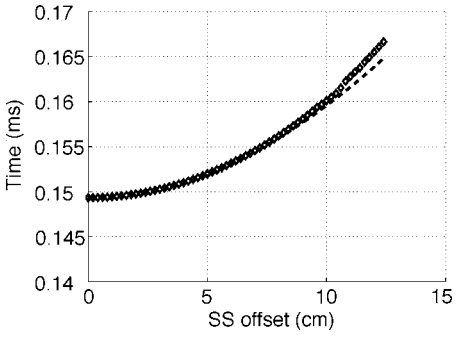

Figure 12. SS-wave traveltime computed using the PP + PS = SS method (rombs) as a function of the SS-wave offset. The dashed line corresponds to the best-fit hyperbola with a moveout velocity of 1780 m/s.

Δx_{PS}. However, we prefer to operate with the function $\Delta x_{PS}(x_{SS})$, which helps to obtain more accurate parameter estimates in the presence of noise (Dewangan and Tsvankin, 2006b).

Model vector **m** includes the five relevant TTI parameters and the layer thickness z:

$$\mathbf{m} \equiv \{V_{P0}, V_{S0}, \epsilon, \delta, \nu, z\}, \tag{6}$$

where V_{P0} and V_{S0} are the velocities of P- and S-waves (respectively) in the symmetry direction, ϵ and δ are Thomsen anisotropy parameters, and ν (tilt) is the angle between the symmetry axis and the vertical. To estimate the elements of **m**, we applied the nonlinear inversion algorithm discussed in Dewangan and Tsvankin (2006a), with the misfit (objective) function given by

$$\mathcal{F} \equiv \frac{(V_{\mathrm{nmo},P}^{\mathrm{calc}} - V_{\mathrm{nmo},P}^{\mathrm{meas}})^2}{(V_{\mathrm{nmo},P}^{\mathrm{meas}})^2} + \frac{(V_{\mathrm{nmo},S}^{\mathrm{calc}} - V_{\mathrm{nmo},S}^{\mathrm{meas}})^2}{(V_{\mathrm{nmo},S}^{\mathrm{meas}})^2} + \frac{(t_{P0}^{\mathrm{calc}} - t_{P0}^{\mathrm{meas}})^2}{(t_{P0}^{\mathrm{meas}})^2} + \frac{(t_{S0}^{\mathrm{calc}} - t_{S0}^{\mathrm{meas}})^2}{(t_{S0}^{\mathrm{meas}})^2} + \frac{\sum_0^{x_{SS}^{\max}} (\Delta t_{PS}^{\mathrm{calc}} - \Delta t_{PS}^{\mathrm{meas}})^2}{\left(\sum_0^{x_{SS}^{\max}} \Delta t_{PS}^{\mathrm{meas}}\right)^2} + \frac{\sum_0^{x_{SS}^{\max}} (\Delta x_{PS}^{\mathrm{calc}} - \Delta x_{PS}^{\mathrm{meas}})^2}{\left(\sum_0^{x_{SS}^{\max}} \Delta x_{PS}^{\mathrm{meas}}\right)^2}. \tag{7}$$

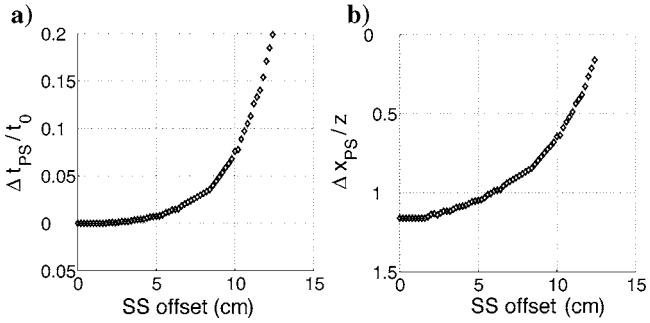

Figure 13. Moveout-asymmetry attributes of the PS-wave computed from equations 3 and 4. (a) Time asymmetry Δt_{PS} normalized by the zero-offset PS-wave time; (b) the corresponding offset asymmetry Δx_{PS} (the projection of $\Delta \boldsymbol{x}_{PS}$ onto the x_1-axis) normalized by the layer thickness.

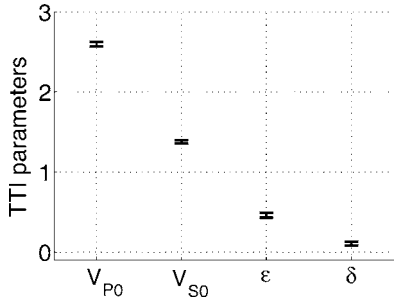

Figure 14. Thomsen parameters of the sample estimated from 2D PP and PS data in the symmetry-axis plane (the velocities are in km/s). Mean values are V_{P0} = 2.6 km/s, V_{S0} = 1.38 km/s, ϵ = 0.46, and δ = 0.11. The estimated tilt of the symmetry axis and layer thickness (not shown) are $\nu = 70°$ and z = 10.9 cm. Standard deviations (marked by the error bars) are 2% for V_{P0}, V_{S0}, and z, 0.03 for ϵ and δ, and 1° for ν.

The superscripts "calc" and "meas" denote the calculated and measured quantities (respectively), and $x_{SS}^{\max}$ is the maximum offset of the constructed SS-wave that corresponds to the offset-to-depth ratio of the recorded PP data close to two.

Initial guesses for the vertical velocities and anisotropy coefficients were based on the isotropic relationships,

$$\begin{aligned} V_{P0} &= V_{\mathrm{nmo},P} = 2.35 \text{ km/s}, \\ V_{S0} &= V_{\mathrm{nmo},S} = 1.78 \text{ km/s}, \quad \epsilon = 0, \quad \delta = 0, \\ z &= V_{\mathrm{nmo},P} t_{P0}/2 = 7.52 \text{ cm}. \end{aligned} \tag{8}$$

The initial tilt of the symmetry axis was randomly chosen between 50° and 85°. Although both the tilt ν and thickness z were known, they were estimated from the data to simulate a field experiment.

To assess the stability of the inversion, the algorithm was applied to multiple realizations of the input PP and PS traveltimes contaminated by random Gaussian noise with zero mean. The standard deviation of the noise was equal to 1/8 of the dominant period, which was assumed to be close to the accuracy of the traveltime picking. Inversion results for 200 realizations of the Gaussian noise are shown in Figure 14. The best-constrained parameter combination is the difference between ϵ and δ, which controls both the time and offset asymmetry (Dewangan and Tsvankin, 2006a). Note that the sample is strongly anisotropic, with the value of ϵ approaching 0.5.

PP- and PS-wave traveltimes computed for the estimated model are practically indistinguishable from the picked traveltimes (Figures 5 and 9) at all offsets. Another indication of the high accuracy of the inversion procedure is that the errors in the known values of ν and z are almost negligible.

TRANSMISSION/CALIBRATION EXPERIMENT

To verify the estimated model using an independent data set, we conducted a transmission experiment on the same sample. The P-wave (vertical) source transducer was fixed at the bottom of the model, while the laser vibrometer scanned the top with a regular interval of 2 mm. The experiment was set up in such a way that traveltimes could be measured for the full range of propagation angles (0°–90°) from the symmetry axis.

Dellinger and Vernik (1994) show that laboratory experiments employing transducers of relatively large size may yield measurements of phase, not group velocity. Our transducer, however, was small (1.5 cm) compared to the thickness of the model (10.8 cm), so the traveltimes should be determined by the corresponding group velocities. Therefore, to reproduce the results of the transmission experiment, we computed the group velocity V_G and the group angle ϕ for the inverted model using the standard TI equations (e.g., Tsvankin, 2001):

$$V_G = V\sqrt{1 + \left(\frac{1}{V}\frac{dV}{d\theta}\right)^2}; \tag{9}$$

$$\tan\phi = \frac{\tan\theta + \dfrac{1}{V}\dfrac{dV}{d\theta}}{1 - \dfrac{\tan\theta}{V}\dfrac{dV}{d\theta}}, \tag{10}$$

where V and θ are the phase velocity and phase angle. It was assumed that ray bending was negligible, and the group angle ϕ corresponds to the source-receiver line.

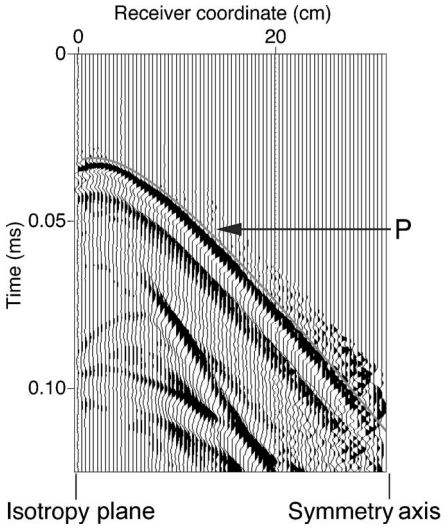

Figure 15. Transmitted wavefield excited by the P-wave transducer and recorded with the laser vibrometer at the top of the model. The receiver moves from a direction approximately perpendicular to the symmetry axis (i.e, from the isotropy plane) to one parallel to the symmetry axis. The solid line is the P-wave traveltime modeled using the inverted parameters from Figure 14.

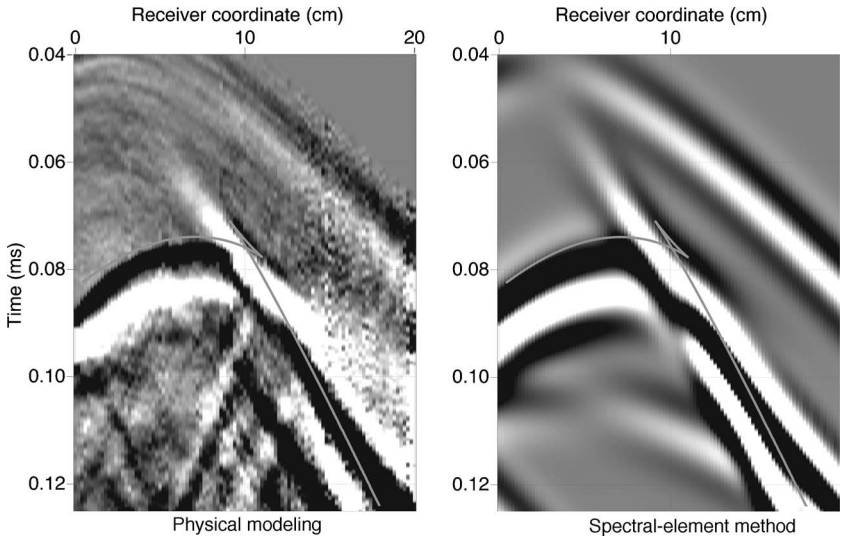

Figure 16. Cusp (triplication) in the transmitted wavefield excited by a shear-wave source. Wavefield recorded by the laser vibrometer (left) is simulated with the spectral-element method for the inverted model in Figure 14 (right). The solid line is the direct shear-wave traveltime computed from the SV-wave group-velocity surface for the inverted model.

Figure 15 shows the raw transmission data, with the zero- and far-offset receiver positions corresponding to the directions approximately perpendicular and parallel (respectively) to the symmetry axis. The first break is the direct P-wave followed by the relatively weak direct S-wave. A solid line marks the P-wave arrival time computed for the inverted TTI model using equations 9 and 10. Evidently, the estimated model parameters accurately predict the P-wave velocity in the transmission experiment, which includes a wider range of propagation directions compared to the reflection data set.

It is interesting that the wavefront of the direct S-wave arrival in Figure 15 exhibits a cusp (triplication) at oblique angles with the symmetry axis. Existence and size of the cusp is mostly governed by the magnitude of the anisotropic parameter $\sigma \equiv (V_{P0}/V_{S0})^2(\epsilon - \delta)$ (Tsvankin, 2001; Thomsen and Dellinger, 2003) that reaches 1.24 for our model. While SV-wave cusps in TI media are well understood theoretically, their experimental observations are rare (e.g., Slater et al., 1993).

To identify the cusp more clearly and measure the transmitted shear-wave traveltimes, we performed another transmission experiment, this time with the S-wave (horizontal) transducer as the source (Figure 16). The transmitted wavefield was also computed for the inverted TTI model from Figure 14 using the spectral-element method (Komatitsch and Vilotte, 1998; Komatitsch et al., 2002). Although the spectral-element code is 2D and cannot be expected to accurately reproduce the recorded amplitudes, the agreement between the measured and modeled wavefields in Figure 16 is excellent.

The spatial extent of the cusp in Figure 16 is significantly larger than that predicted by the group-velocity surface (i.e., by ray-theory modeling). This is consistent with the observation by Martynov and Mikhailenko (1984) that ray theory underestimates the actual size of the SV-wave cusp in TI media. The reflected PS data analyzed above do not exhibit cuspoidal behavior because the shear-wave group angles corresponding to the cusp are not reached during the P-to-S conversion at the bottom of the layer.

Ray-theoretical S-wave traveltimes computed for the inverted model (solid lines) fail to match the observed arrivals not just in the area of the cusp, but also at large offsets. To explain this discrepancy, we increased the frequency of the signal used in the spectral-element modeling (Figure 17). The higher-frequency wavefield shows two distinct arrivals with close traveltimes — the direct S-wave and the refracted P-wave. Interference of these waves on the lower-frequency section (Figure 16) produces a complicated wavelet that arrives ahead of the direct shear wave at large offsets. Another wave more clearly visible in Figure 17 is the P-wave multiple in the layer.

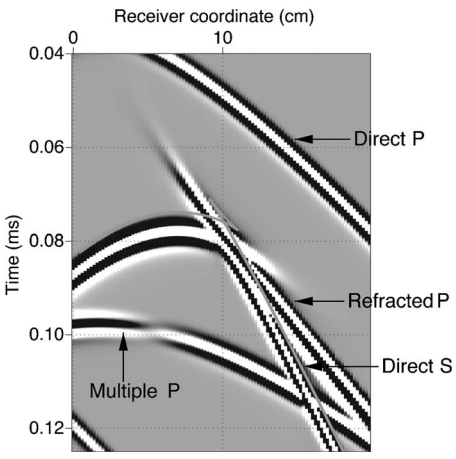

Figure 17. Same as the simulated wavefield (right section) in Figure 16, but the spectral-element modeling was performed with a higher-frequency wavelet.

DISCUSSION AND CONCLUSIONS

To estimate anisotropy parameters from reflection data, P-wave moveout can be combined with converted PS-waves. We performed traveltime inversion of 2D multicomponent physical-modeling data recorded over a phenolic sample manufactured to simulate a horizontal TI layer with a large (70°) tilt of the symmetry axis.

Long-offset PP-waves and converted (PS and SP) modes were acquired in the symmetry-axis plane of the material and processed using the modified PP + PS = SS method developed in Dewangan and Tsvankin (2006a). In addition to the traveltimes of the pure SS reflections (which are not excited in the survey), this methodology produces the moveout-asymmetry attributes of the PS arrivals. Our case study confirms the conclusion of Dewangan and Tsvankin (2006a) that the combination of the PS-wave time and offset asymmetry attributes with the NMO velocities and zero-offset times of the PP- and SS-waves makes it possible to estimate the pertinent Thomsen parameters, the tilt of the symmetry axis, and the layer thickness.

The sample proved to be strongly anisotropic, with the magnitude of P-wave velocity variations approaching 50% ($\epsilon = 0.46$, $\delta = 0.11$) and large positive anellipticity ($\eta = 0.29$). The inversion algorithm gave accurate estimates of the known values of the tilt of the symmetry axis and layer thickness. To verify the parameter-estimation results, we conducted a transmission experiment using both P-wave and S-wave transducers. The P-wave group-velocity curve computed for the inverted model accurately matched the first breaks of the transmitted P-wave.

The wavefront of the transmitted SV-wave has a more complicated shape, with a cusp (triplication) between the symmetry axis and the isotropy plane. Although the observed cusp is noticeably wider than that predicted by the group-velocity surface calculated for the estimated model, this discrepancy is caused by the inadequacy of ray theory in describing triplications. More accurate modeling using the spectral-element method allowed us to reproduce the cusp and all other major features of the transmitted wavefield excited by the shear transducer. Because the shape and spatial extent of SV-wave cusps are highly sensitive to the medium parameters, the excellent agreement between the recorded wavefield and the modeling results confirms the robustness of our inversion method.

Note that in field experiments, the azimuth of the symmetry axis has to be estimated from the polarization of PS-waves or the azimuthal variation of such signatures as NMO velocities and AVO (amplitude variation with offset) gradients. Also, beause our algorithm is designed for a single TTI layer, in field-data applications it must be combined with the layer-stripping technique discussed by Dewangan and Tsvankin (2006c).

ACKNOWLEDGMENTS

We are grateful to members of the A(nisotropy)-Team of the Center for Wave Phenomena (CWP), Colorado School of Mines (CSM), for helpful discussions and to Ken Larner (CSM) and the GEOPHYSICS reviewers for their careful reviews of the manuscript. We thank Jean-Paul Ampuero (ETH Hoenggerberg) for making his spectral-

element code available to us. Support for this research was provided by the Consortium Project on Seismic Inverse Methods for Complex Structures at CWP and by the Chemical Sciences, Geosciences and Biosciences Division, Office of Basic Energy Sciences, Office of Science, U. S. Department of Energy. Experimental work was supported by the National Science Foundation (EAR-0111804, EAR-0337379) and the Army Research Office (DAAG55-98-1-0277, DAAD19-03-1-0292).

REFERENCES

Angerer, E., S. A. Horne, J. E. Gaiser, R. Walters, S. Bagala, and L. Vetri, 2002, Characterization of dipping fractures using PS mode-converted data: 72nd Annual International Meeting, SEG, Expanded Abstracts, 1010–1013.

Dellinger, J., and L. Vernik, 1994, Do traveltimes in pulse-transmission experiments yield anisotropic group or phase velocities?: Geophysics, **59**, 1774–1779.

Dewangan, P., and I. Tsvankin, 2006a, Modeling and inversion of PS-wave moveout asymmetry for tilted TI media: Part I — Horizontal TTI layer: Geophysics, this issue.

———, 2006b, Modeling and inversion of PS-wave moveout asymmetry for tilted TI media: Part II — Dipping TTI layer: Geophysics, this issue.

———, 2006c, Velocity-independent layer stripping of PP and PS reflection traveltimes: Geophysics, this issue.

Ebrom, D., J. McDonald, and R. Tatham, 1992, Sideswipe in a 3-D, 3-C model survey: The Leading Edge, **11**, 45–51.

Grechka, V., and P. Dewangan, 2003, Generation and processing of pseudo shear-wave data: Theory and case study: Geophysics, **68**, 1807–1816.

Grechka, V., and I. Tsvankin, 2000, Inversion of azimuthally dependent NMO velocity in transversely isotropic media with a tilted axis of symmetry: Geophysics, **65**, 232–246.

———, 2002, PP + PS = SS: Geophysics, **67**, 1961–1971.

Grechka, V., A. Pech, and I. Tsvankin, 2002, Multicomponent stacking-velocity tomography for transversely isotropic media: Geophysics, **67**, 1564–1574.

Grechka, V., S. Theophanis, and I. Tsvankin, 1999, Joint inversion of P- and PS-waves in orthorhombic media, Theory and a physical modeling study: Geophysics, **64**, 146–161.

Helbig, K., 1994, Foundations of elastic anisotropy for exploration seismics: Pergamon Press, Inc.

Isaac, J. H., and D. C. Lawton, 1999, Image mispositioning due to dipping TI media: A physical seismic modeling study: Geophysics, **64**, 1230–1238.

Komatitsch, D., and J. P. Vilotte, 1998, The spectral-element method: An efficient tool to simulate the seismic response of 2D and 3D geological structures: Bulletin of the Seismological Society of America, **88**, 368–392.

Komatitsch, D., J. Ritsema, and J. Tromp, 2002, The spectral-element method, Beowulf computing, and global seismology: Science, **298**, 1737–1742.

Martynov, V. N., and B. G. Mikhailenko, 1984, Numerical modelling of elastic waves in anisotropic inhomogeneous media for the halfspace and the sphere: Geophysical Journal of the Royal Astronomical Society, **76**, 53–63.

Nishizawa, O., T. Satoh, X. Lei, and Y. Kuwahara, 1997, Laboratory studies of seismic wave propagation in inhomogeneous media using a laser doppler vibrometer: Bulletin of the Seismological Society of America, **87**, 809–823.

Rathore, J. S., E. Fjaer, R. M. Holt, and L. Renlie, 1995, P- and S-wave anisotropy of a synthetic sandstone with controlled crack geometry: Geophysical Prospecting, **43**, 711–728.

Scales, J. A., and K. van Wijk, 1999, Multiple scattering attenuation and anisotropy of ultrasonic surface waves: Applied Physics Letters, **74**, 3899–3901.

Slater, C., S. Crampin, L. Y. Brodov, and V. M. Kuznetsov, 1993, Observations of anisotropic cusps in transversely isotropic clay: Canadian Journal of Exploration Geophysics, **29**, 216–226.

Thomsen, L., 1986, Weak elastic anisotropy: Geophysics, **51**, 1954–1966.

Thomsen, L., and J. Dellinger, 2003, On shear-wave triplication in transversely isotropic media: Journal of Applied Geophysics, **54**, 289–296.

Tsvankin, I., 1997, Reflection moveout and parameter estimation for horizontal transverse isotropy: Geophysics, **62**, 614–629.

———, 2001, Seismic signatures and analysis of reflection data in anisotropic media: Elsevier Science Publishing Company, Inc.

Tsvankin, I., and V. Grechka, 2000, Dip moveout of converted waves and parameter estimation in transversely isotropic media: Geophysical Prospecting, **48**, 257–292.

Vestrum, R. W., D. C. Lawton, and R. Schmid, 1999, Imaging structures below dipping TI media: Geophysics, **64**, 1239–1246.